This is the accepted manuscript made available via CHORUS. The article has been published as:

Metasurface-Based Solid Poincaré Sphere Polarizer

Shuai Wang, Shun Wen, Zi-Lan Deng, Xiangping Li, and Yuanmu Yang

Phys. Rev. Lett. **130**, 123801 — Published 23 March 2023

DOI: 10.1103/PhysRevLett.130.123801

Metasurface-based solid Poincaré sphere polarizer

Shuai Wang[1], Shun Wen[1], Zi-Lan Deng[2,*], Xiangping Li[2], Yuanmu Yang[1,*]

[1]State Key Laboratory for Precision Measurement Technology and Instruments, Department of Precision Instrument, Tsinghua University, Beijing 100084, China

[2]Guangdong Provincial Key Laboratory of Optical Fiber Sensing and Communications, Institute of Photonics Technology, Jinan University, Guangzhou 510632, China.

The combination of conventional polarization optical elements, such as linear polarizers and waveplates, is widely adopted to tailor light's state of polarization (SoP). Meanwhile, less attention has been given to the manipulation of light's degree of polarization (DoP). Here, we propose metasurface-based polarizers that can filter unpolarized incident light to light with any prescribed SoP and DoP, corresponding to arbitrary points located both at the surface and within the solid Poincaré sphere. The Jones matrix elements of the metasurface are inverse-designed via the adjoint method. As prototypes, we experimentally demonstrated metasurface-based polarizers in near-infrared frequencies that can convert unpolarized light into linear, elliptical, or circular polarizations with varying DoPs of 1, 0.7, and 0.4, respectively. Our work unlocks a new degree of freedom for metasurface polarization optics and may break new ground for a variety of DoP-related applications, such as polarization calibration and quantum state tomography.

The manipulation of the polarization of light is of great importance in the optics community. Conventional polarization optical elements focus on the manipulation of the state of polarization (SoP) of fully polarized light corresponding to a point at the surface of the Poincaré sphere. The Poincaré sphere is widely used to graphically represent the SoP in terms of its orientation angle and ellipticity angle. For instance, a linear polarizer, as the most widely adopted polarization-selective element, can convert an unpolarized incident beam to a beam with linear SoP, corresponding to points at the

equator of the Poincaré sphere, as schematically shown in Fig. 1(a). To generate an elliptically or circularly polarized light, one typically needs to utilize the cascade of a linear polarizer and a waveplate.

Beyond the manipulation of fully polarized light, controlling the degree of polarization (DoP) of light can also be of particular importance in many fields. DoP defines the purity of polarization. For fully polarized and unpolarized light, the DoP is defined as 1 and 0, respectively, while for partially polarized light, the DoP varies between 0 and 1. To graphically represent the DoP, one can resort to a solid unit Poincaré sphere of which the radial coordinates can be employed to directly represent the DoP [1]. In this way, partially polarized light is represented by the point inside the Poincaré sphere. In many polarization-related optical applications, pure SoP manipulation is not sufficient. The additional maneuvering of DoP is highly desired in both quantum and classic regimes. For example, the partial polarizer and wedge depolarizer are used to control the output polarization of the entangled photons, leading to the generations of Werner states and maximally entangled mixed states in quantum optics [2-5]. The precise control of SoP and DoP is also crucial for the calibration of polarimetric metrology systems [6,7], often applied in the characterization of liquid crystal on silicon devices [8], ellipsometry [9], and remote sensing [10]. The DoP of light can be controlled by either depolarizing a polarized beam or partially polarizing an unpolarized beam. The working principle of the depolarizer is based on the incoherent superposition of different SoPs encoded in the time [7], space [11], or frequency domain [12]. Moreover, a birefringent metamaterial-based partial polarizer has been proposed by controlling the transmittance of light with two orthogonal linear polarization states [13]. Up to now, the simultaneous and independent manipulation of DoP and SoP generally requires the superposition of two orthogonal polarization states with different weights in a bulky system composed of multiple polarizing beam splitters, mirrors, and waveplates, resulting in a large form factor and high complexity [14].

On the other hand, it has been shown that a new class of subwavelength optical elements, metasurface [15-25], may serve as an ultra-compact and versatile platform to

manipulate the amplitude [26-30], phase [31-35], and polarization [35-43] of light over a short light propagation distance. Specifically, for polarization manipulation, waveplate-type metasurface based on birefringence has been proposed for arbitrary SoP conversion [35,42,43]. Furthermore, it has been shown that the large design degree of freedom of the metasurface can allow the simultaneous generation of arbitrary assembly of SoP [40,41]. On the other hand, polarizer-type metasurfaces based on dichroism have also been exploited. In 2009, a broadband circular polarizer that can directly convert an unpolarized light to circular polarization was demonstrated based on a 3D gold helix metasurface [44]. In 2021, a diatomic silicon nano-antenna-based metasurface was shown to be capable of converting an unpolarized light to any SoP, including linear, elliptical, and circular polarizations, corresponding to arbitrary points at the surface of the Poincaré sphere [45], as schematically shown in Fig. 1(b). The generation of light with arbitrary SoP and DoP in a miniaturized platform remains elusive.

Facing this challenge, here we propose and experimentally demonstrate metasurface-based polarizers that can convert an unpolarized near-infrared beam into a beam with any combination of SoP and DoP, as schematically depicted in Fig. 1(c). Since the polarization of the output beam can be located at arbitrary points over the solid Poincaré sphere, we name such a device “solid Poincaré sphere polarizer”. The difference in the generated polarization between a linear polarizer, a surface Poincaré sphere polarizer, and a solid Poincaré sphere polarizer is graphically illustrated in Fig. 1(d). The generation of arbitrary SoP and DoP from an unpolarized beam, composed of arbitrary orthogonal polarization states without fixed phase difference, is made possible by independently controlling the transmittance of two orthogonally polarized light beams impinging on the metasurface. To search for structures that uniquely satisfy the Jones matrix requirement for the on-demand and simultaneous DoP and SoP control, we extended the adjoint-based inverse design approach [46-50] by building a complete framework in full Jones matrix under arbitrary polarization basis. We experimentally validate the concept with nine metasurface-based polarizers that convert unpolarized

light into linear, elliptical, or circular polarization with varying DoPs.

The underlying physical mechanism of the simultaneous modulation of DoP and SoP is schematically shown in Fig. 2. An unpolarized beam can be treated as a superposition of two orthogonally polarized beams with random intensity and phase difference δ as [51],

$$\langle \vec{e}_{un} \rangle = \langle \sqrt{S}\vec{\alpha}^{+} + \sqrt{1-S}\vec{\alpha}^{-}e^{i\delta} \rangle, \tag{1}$$

The bracket $\langle\ \rangle$ denotes the time average on a series of random amplitude and phase differences, where the random intensity S belongs to [0, 1] and $\langle S \rangle = 0.5$. The two orthogonal polarization states can be described as,

$$\vec{\alpha}^{+} = \boldsymbol{R}(\psi)\begin{bmatrix}\cos\chi \\ -i\sin\chi\end{bmatrix}, \tag{2}$$

$$\vec{\alpha}^{-} = \boldsymbol{R}(\psi - 90°)\begin{bmatrix}\cos\chi \\ i\sin\chi\end{bmatrix}, \tag{3}$$

where ψ and χ are the orientation angle and the ellipticity angle of polarization, respectively, as schematically illustrated in Fig. 1(d). $\boldsymbol{R}$ is the rotation matrix.

We assume that the metasurface converts the polarization $\vec{\alpha}^{+}$ and $\vec{\alpha}^{-}$ into their handedness-flipped states $\vec{\beta}^{+} = (\vec{\alpha}^{+})^{*}$ and $\vec{\beta}^{-} = (\vec{\alpha}^{-})^{*}$ with different amplitude modulation, the symbol * represents the operation of complex conjugation. The locations of the above-mentioned polarization on the Poincaré sphere are schematized in Fig. 2(b). The two orthogonal polarization states are antipodal (diametrically opposite to each other on a great circle), and the handedness-flipped states $\vec{\alpha}^{+}(\vec{\alpha}^{-})$ and $\vec{\beta}^{+}(\vec{\beta}^{-})$ are mirror symmetric with respect to the equatorial plane.

To construct an output beam with any combination of SoP and DoP, our approach is to combine $\vec{\beta}^{-}$ with a portion of its orthogonal polarization $\vec{\beta}^{+}$ to construct an unpolarized beam. The remaining portion of $\vec{\beta}^{+}$ is a polarized beam, where $\vec{\beta}^{+}$ determines the SoP of the output beam. To simultaneously and independently control the SoP and DoP, we design a metasurface with a Jones matrix,

$$\boldsymbol{J} = \begin{bmatrix} t_{\beta^{+}\alpha^{+}} & t_{\beta^{+}\alpha^{-}} \\ t_{\beta^{-}\alpha^{+}} & t_{\beta^{-}\alpha^{-}} \end{bmatrix} = \begin{bmatrix} 1 & 0 \\ 0 & c \end{bmatrix}. \tag{4}$$

Such a Jones matrix has a polarization base of $\{\vec{\alpha}^{+}, \vec{\alpha}^{-}\}$ in the incident space and

a polarization base of $\{\vec{\beta}^+, \vec{\beta}^-\}$ in the output space, where $t_{\beta\alpha}$ represents the conversion coefficient from the polarization state $\vec{\alpha}$ to $\vec{\beta}$.

Consequently, the output beam can be described as,

$$\langle \vec{e}_{out} \rangle = \langle \sqrt{S}\vec{\beta}^+ + c\sqrt{1-S}\vec{\beta}^- e^{i\delta} \rangle, \tag{5}$$

which results in the intensity of the output beam as,

$$\begin{aligned} \langle I_{out} \rangle &= \langle \vec{e}_{out}^* \vec{e}_{out} \rangle \\ &= (1-|c|^2)\left(\vec{\beta}^+\right)^* \vec{\beta}^+/2 + |c|^2 \langle \vec{e}_{un}^* \vec{e}_{un} \rangle \\ &= (1+|c|^2)/2, \end{aligned} \tag{6}$$

where the term $(1-|c|^2)\left(\vec{\beta}^+\right)^* \vec{\beta}^+/2$ represents the polarized part in the output beam with an SoP of $\vec{\beta}^+$. $|c|^2 \langle \vec{e}_{un}^* \vec{e}_{un} \rangle$ represents the unpolarized part, which is an incoherent superposition of $\vec{\beta}^-$ and $\vec{\beta}^+$ with random intensity. The DoP of the output beam can be described as,

$$\text{DoP} = (1-|c|^2)/(1+|c|^2). \tag{7}$$

The transmittance matrices are used to describe the metasurface-based polarizer, which can be described as,

$$\boldsymbol{T} = \boldsymbol{J} \odot \boldsymbol{J}^* = \begin{bmatrix} T_{\beta^+\alpha^+} & T_{\beta^+\alpha^-} \\ T_{\beta^-\alpha^+} & T_{\beta^-\alpha^-} \end{bmatrix} = \begin{bmatrix} 1 & 0 \\ 0 & |c|^2 \end{bmatrix}, \tag{8}$$

where $\odot$ denotes Hadamard product.

To realize the desired transmittance matrices as specified in Eq. (8), we designed polarization-sensitive metasurfaces via adjoint-based topology optimization [43,46]. The metasurface consists of a square array of 600-nm-tall silicon nanostructures with a period of 860 nm sitting on a 650-μm-thick sapphire substrate. The 600-nm-tall silicon meta-atom may induce enough anisotropy for polarization manipulation at the targeted operation wavelength of around 1150 nm. The period is set to be smaller than the operating wavelength to avoid high-order diffraction. We define the Figure-of-Merit (FoM) of the optimization as,

$$\mathrm{FoM} = \sum_{i\in\{\vec{\alpha}^+,\vec{\alpha}^-\}}\sum_{j\in\{\vec{\beta}^+,\vec{\beta}^-\}}\left|T'_{ji} - T_{ji}\right|, \quad (9)$$

where T'_{ji} and T_{ji} are the targeted and calculated transmittance at the operation wavelength of 1150 nm, respectively. To reduce the FoM, we ran both a forward and an adjoint electromagnetic simulation in each iteration of the optimization. The evolution of the shape of the nanostructure (the dielectric constant at each specific location of the metasurface unit cell) is governed by the inner product of the electromagnetic fields generated from the forward and adjoint simulation.

Figure 3(a) shows the FoM over the course of the optimization process for a metasurface-based linear polarizer with DoP of 1, 0.7, and 0.4, respectively. The inset shows the converged shape of the silicon nano-antenna at the end of the optimization. We further designed elliptical [$\psi = 0$, $\chi = 22.5^\circ$] and right circular polarizers with varying DoPs using an identical strategy, with results shown in Figs. 3(b), (c), respectively. The Stokes parameters are employed to characterize the polarization of the output beam through the metasurface-based polarizer with a DoP of 0.7 as shown in Figs. 3(d-f). The DoP approaches 0.6 at the end of the optimization process, deviating from the desired value of 0.7. The reason for the discrepancy between the optimized and desired DoP is that in the practical physical system made of silicon-based meta-atoms with a sapphire substrate, it is difficult to optimize $T_{\beta^+\alpha^+}$ to the target value of 100%. The decreased $T_{\beta^+\alpha^+}$ lead to the decrease of the output DoP, which could be further improved by setting compromised efficiency target. The Stokes parameters of the output beams can be subsequently obtained from the analysis of the Mueller matrix of the metasurface [52]. The underlying physical principle of the polarization dichroism of the optimized metasurface can be analyzed by the multipole mode decomposition method [52].

To experimentally validate the design of solid Poincaré sphere polarizers, we fabricated nine metasurfaces with targeted responses corresponding to linear, elliptical, and circular polarizers with varying DoPs of 1, 0.7, and 0.4, respectively. The fabrication of the metasurface is based on the standard electron-beam lithography and

reactive-ion etching process, thus being compatible with the scalable complementary metal-oxide-semiconductor process. The scanning electron microscopy (SEM) images of the metasurface unit cells are shown in the inset of Fig. 4.

The experimental setup for characterizing the Stokes parameters of the output beam transmitted from various metasurfaces is illustrated in Fig. 4(a). The light source is a halogen-tungsten lamp, with its DoP measured to be near zero in the wavelength range from 1100 nm to 1200 nm [52]. The experimentally measured output polarization of the nine metasurface-based polarizers is represented in the Poincaré sphere and compared with the designed case, as illustrated in Figs. 4(b)-(d). The discrepancies in the response of the measured and designed metasurface-based polarizers are quantified by the Euclidean distance in the Poincaré sphere, defined as,

$$d = \sqrt{(S_1' - S_1)^2 + (S_2' - S_2)^2 + (S_3' - S_3)^2}\ , \tag{10}$$

where $[S_1, S_2, S_3]^T$ and $[S_1', S_2', S_3']^T$ are measured and designed Stokes parameters, respectively. The measured Stokes parameters agree closely with the design, with the discrepancy summarized in Table Ⅰ. The discrepancy is most likely a result of fabrication imperfection, The working wavelength may be extended to a broadband range by utilizing a multi-wavelength inverse design scheme [52] or by using geometric phase metasurfaces [39,47]. The analysis on metasurface-based polarizers' tolerance to fabrication error is also provided in the Supplemental Material [52].

TABLE Ⅰ. Experimental characterization of metasurface-based solid Poincaré sphere polarizer

DoP / SoP	1	0.7	0.4
Linear	0.11@1150 nm	0.03@1149 nm	0.10@1151 nm
Elliptical	0.19@1190 nm	0.03@1166 nm	0.07@1131 nm
Circular	0.16@1132 nm	0.12@1164 nm	0.03@1133 nm

In conclusion, we have proposed and demonstrated metasurface-based solid Poincaré sphere polarizers that can convert an unpolarized incident beam to a

polarization located at an arbitrary point within the solid Poincaré sphere. To design a polarizer that can control both SoP and DoP, a strategy involving the delicate engineering of the Jones matrix of the metasurface that applies to unpolarized incident light has been developed. The metasurface has a freeform structure designed via the synergy of Jones matrix analysis and iterative optimization by the adjoint method. The metasurface-based Solid Poincaré sphere polarizer allows the generalized manipulation of the DoP and SoP of the incident light. It may also be possible to generate an arbitrary assembly of SoP and DoP leveraging multiple diffraction orders in a polarization-dependent meta-grating [37,40] with a multi-order inverse design scheme as described in [52]. Combining with the metasurface's design flexibility to spatially manipulate the amplitude and phase of light at a subwavelength resolution, one may utilize the solid Poincaré sphere polarizer to generate complex classical or quantum light states with an additional degree of freedom for a variety of applications, including imaging, communication, and information encryption.

This work was supported by the National Natural Science Foundation of China (62135008, 61975251, 62075084), the Guoqiang Institute, Tsinghua University, and the Guangdong Basic and Applied Basic Research Foundation (2022B1515020004). We acknowledge Dr. Wei Liu at the National Defense University of Technology for the fruitful discussion.

*Corresponding authors.
zilandeng@jnu.edu.cn
ymyang@tsinghua.edu.cn

[1] M. Born and E. Wolf, *Principles of Optics* (Cambridge University Press, Cambridge, 2019).
[2] G. Puentes, D. Voigt, A. Aiello, and J. P. Woerdman, Opt Lett **31**, 2057 (2006).
[3] N. A. Peters, J. B. Altepeter, D. Branning, E. R. Jeffrey, T.-C. Wei, and P. G. Kwiat, Phys. Rev. Lett. **92**, 133601 (2004).
[4] A. Shaham and H. S. Eisenberg, Opt. Lett. **37**, 2643 (2012).
[5] T.-C. Wei, J. B. Altepeter, D. Branning, P. M. Goldbart, D. F. V. James, E. Jeffrey, P. G. Kwiat, S. Mukhopadhyay, and N. A. Peters, Phys. Rev. A **71**, 032329 (2005).
[6] A. B. Mahler and R. A. Chipman, Appl. Opt. **50**, 1726 (2011).
[7] A. Peinado, A. Lizana, and J. Campos, Opt. Lett. **39**, 659 (2014).
[8] A. Márquez, I. Moreno, C. Iemmi, A. Lizana, J. Campos, and M. J. Yzuel, Opt. Express **16**, 1669 (2008).
[9] H. Tompkins and E. A. Irene, *Handbook of ellipsometry* (William Andrew, 2005).
[10] W. Egan, *Polarization in remote sensing* (SPIE, 1992).
[11] R. H. Hughes, Rev. Sci. Instrum **31**, 1156 (1960).
[12] W. Burns, J. Lightwave Technol. **1**, 475 (1983).
[13] S. Maurya, M. Nyman, M. Kaivola, and A. Shevchenko, Opt. Express **27**, 27335 (2019).
[14] A. Lizana, I. Estevez, F. A. Torres-Ruiz, A. Peinado, C. Ramirez, and J. Campos, Opt. Lett. **40**, 3790 (2015).
[15] N. Yu, P. Genevet, M. A. Kats, F. Aieta, J. P. Tetienne, F. Capasso, and Z. Gaburro, Science **334**, 333 (2011).
[16] Q. Song, X. Liu, C.-W. Qiu, and P. Genevet, Appl. Phys. Rev **9**, 011311 (2022).
[17] H.-H. Hsiao, C. H. Chu, and D. P. Tsai, Small Methods **1**, 1600064 (2017).
[18] H.-T. Chen, A. J. Taylor, and N. Yu, Rep. Prog. Phys **79**, 076401 (2016).
[19] P. Genevet, F. Capasso, F. Aieta, M. Khorasaninejad, and R. Devlin, Optica **4**, 139 (2017).
[20] A. S. Solntsev, G. S. Agarwal, and Y. S. Kivshar, Nat. Photonics **15**, 327 (2021).
[21] C.-W. Qiu, T. Zhang, G. Hu, and Y. Kivshar, Nano Lett. **21**, 5461 (2021).
[22] A. C. Overvig, S. A. Mann, and A. Alù, Phys. Rev. X **11**, 021050 (2021).
[23] H. Ren *et al.*, Nat. Commun. **10**, 2986 (2019).
[24] R.-H. Fan, B. Xiong, R.-W. Peng, and M. Wang, Adv. Mater. **32**, 1904646 (2020).
[25] K. Wang *et al.*, Science **361**, 1104 (2018).
[26] G. Y. Lee, G. Yoon, S. Y. Lee, H. Yun, J. Cho, K. Lee, H. Kim, J. Rho, and B. Lee, Nanoscale **10**, 4237 (2018).
[27] Q. Fan *et al.*, Phys. Rev. Lett. **125**, 267402 (2020).
[28] A. C. Overvig, S. Shrestha, S. C. Malek, M. Lu, A. Stein, C. Zheng, and N. Yu, Light Sci. Appl. **8**, 92 (2019).
[29] A. Overvig, N. Yu, and A. Alù, Phys. Rev. Lett. **126**, 073001 (2021).
[30] M. Liu *et al.*, Light Sci. Appl. **10**, 107 (2021).

[31] G. Zheng, H. Muhlenbernd, M. Kenney, G. Li, T. Zentgraf, and S. Zhang, Nat. Nanotechnol. **10**, 308 (2015).
[32] J. P. Balthasar Mueller, N. A. Rubin, R. C. Devlin, B. Groever, and F. Capasso, Phys. Rev. Lett. **118**, 113901 (2017).
[33] L. Huang, X. Chen, H. Muhlenbernd, G. Li, B. Bai, Q. Tan, G. Jin, T. Zentgraf, and S. Zhang, Nano Lett. **12**, 5750 (2012).
[34] Y. Yuan, K. Zhang, B. Ratni, Q. Song, X. Ding, Q. Wu, S. N. Burokur, and P. Genevet, Nat. Commun. **11**, 4186 (2020).
[35] Y. Yang, W. Wang, P. Moitra, Kravchenko, II, D. P. Briggs, and J. Valentine, Nano Lett. **14**, 1394 (2014).
[36] A. H. Dorrah, N. A. Rubin, A. Zaidi, M. Tamagnone, and F. Capasso, Nat. Photonics **15**, 287 (2021).
[37] N. A. Rubin, G. D'Aversa, P. Chevalier, Z. Shi, W. T. Chen, and F. Capasso, Science **365**, eaax1839 (2019).
[38] Z. L. Deng *et al.*, Nano Lett. **18**, 2885 (2018).
[39] Q. Song *et al.*, Nat. Commun. **12**, 3631 (2021).
[40] Y.-J. Gao, X. Xiong, Z. Wang, F. Chen, R.-W. Peng, and M. Wang, Phys. Rev. X **10**, 031035 (2020).
[41] Y.-J. Gao, Z. Wang, Y. Jiang, R.-W. Peng, Z.-Y. Wang, D.-X. Qi, R.-H. Fan, W.-J. Tang, and M. Wang, Phys. Rev. Lett. **129**, 023601 (2022).
[42] C.-C. Chang, Z. Zhao, D. Li, A. J. Taylor, S. Fan, and H.-T. Chen, Phys. Rev. Lett. **123**, 237401 (2019).
[43] Z. Shi, A. Y. Zhu, Z. Li, Y. W. Huang, W. T. Chen, C. W. Qiu, and F. Capasso, Sci. Adv. **6**, eaba3367 (2020).
[44] J. K. Gansel, M. Thiel, M. S. Rill, M. Decker, K. Bade, V. Saile, G. von Freymann, S. Linden, and M. Wegener, Science **325**, 1513 (2009).
[45] S. Wang, Z. L. Deng, Y. Wang, Q. Zhou, X. Wang, Y. Cao, B. O. Guan, S. Xiao, and X. Li, Light Sci. Appl. **10**, 24 (2021).
[46] D. Sell, J. Yang, S. Doshay, R. Yang, and J. A. Fan, Nano Lett. **17**, 3752 (2017).
[47] A. Y. Piggott, J. Lu, K. G. Lagoudakis, J. Petykiewicz, T. M. Babinec, and J. Vučković, Nat. Photonics **9**, 374 (2015).
[48] Y. Meng *et al.*, Light Sci. Appl. **10**, 235 (2021).
[49] S. Molesky, Z. Lin, A. Y. Piggott, W. Jin, J. Vucković, and A. W. Rodriguez, Nature Photonics **12**, 659 (2018).
[50] M. B. Giles and N. A. Pierce, Flow Turbul Combust **65**, 393 (2000).
[51] A. Shevchenko, M. Roussey, A. T. Friberg, and T. Setälä, Optica **4** (2017).
[52] See Supplemental Material for further theoretical and experimental detail.

Figures and Captions

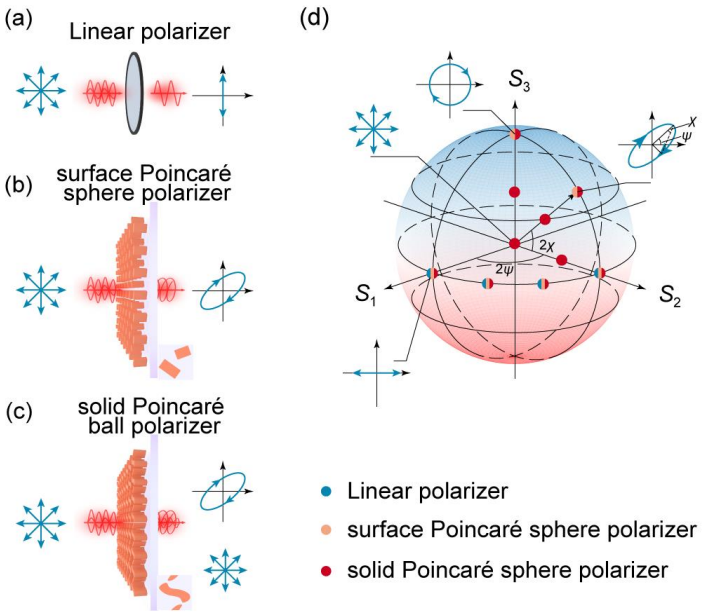

FIG. 1. Comparison of the linear polarizer, surface Poincaré sphere polarizer, and solid Poincaré sphere polarizer. (a) Schematic of a linear polarizer that converts an unpolarized incident beam into linear polarization located at the equator of the Poincaré sphere. (b) Schematic of a surface Poincaré sphere polarizer that converts an unpolarized incident beam into arbitrary polarizations located at the surface of the Poincaré sphere. (c) Schematic of a solid Poincaré sphere polarizer that converts an unpolarized incident beam into arbitrary polarizations located at the surface and within the Poincaré sphere. (d) Schematic of a Poincaré sphere and the locations of output polarization states generated from a linear polarizer, a surface Poincaré sphere polarizer, and a solid Poincaré sphere polarizer, respectively.

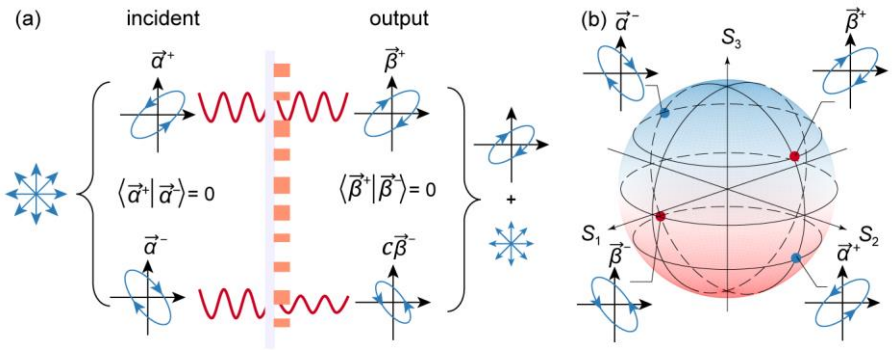

FIG. 2. Physical mechanism for the simultaneous and independent modulation of DoP and SoP. (a) An unpolarized beam can be treated as a superposition of two orthogonal polarization states with random phase differences. The output polarization $\vec{\beta}^-$ combines a portion of its orthogonal polarization $\vec{\beta}^+$ to construct an unpolarized beam with an intensity of $|c|^2$. The remaining portion of $\vec{\beta}^+$ is a polarized beam with an intensity of $(1-|c|^2)/2$. The output is the superposition of the unpolarized and polarized beams, with the ratio controlled by *c*. (b) Schematic illustration of the locations of the polarization states $\vec{\alpha}^+$, $\vec{\alpha}^-$, $\vec{\beta}^+$ and $\vec{\beta}^-$ at the surface of the Poincaré sphere.

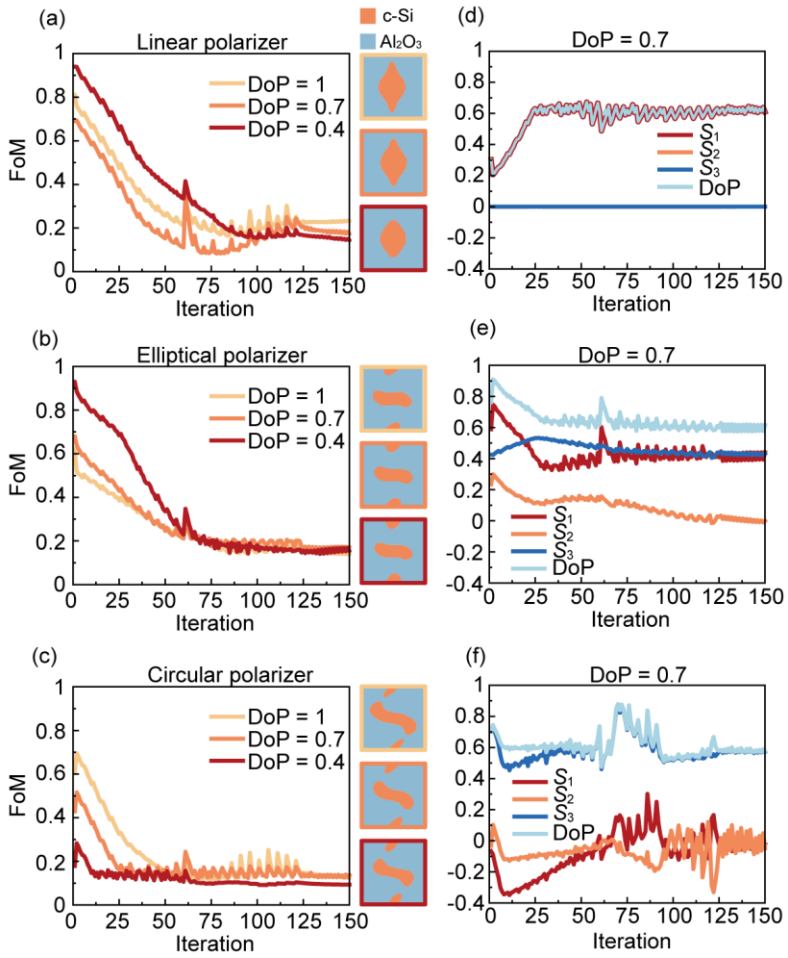

FIG. 3. Inverse design of the metasurface-based solid Poincaré sphere polarizer. (a)-(c) FoM as a function of the iteration for linear (a), elliptical (b), and circular (c) polarizer with DoP of 1, 0.7, and 0.4, respectively. The insets are the antenna shape at the end of the iterative optimization. (d)-(f) Stokes parameter and DoP of output beams transmitted through the metasurface-based linear (d), elliptical (e), and circular (f) polarizers, respectively, with an output DoP of 0.7 under the illumination by the unpolarized incident beam at the designed wavelength of 1150 nm.

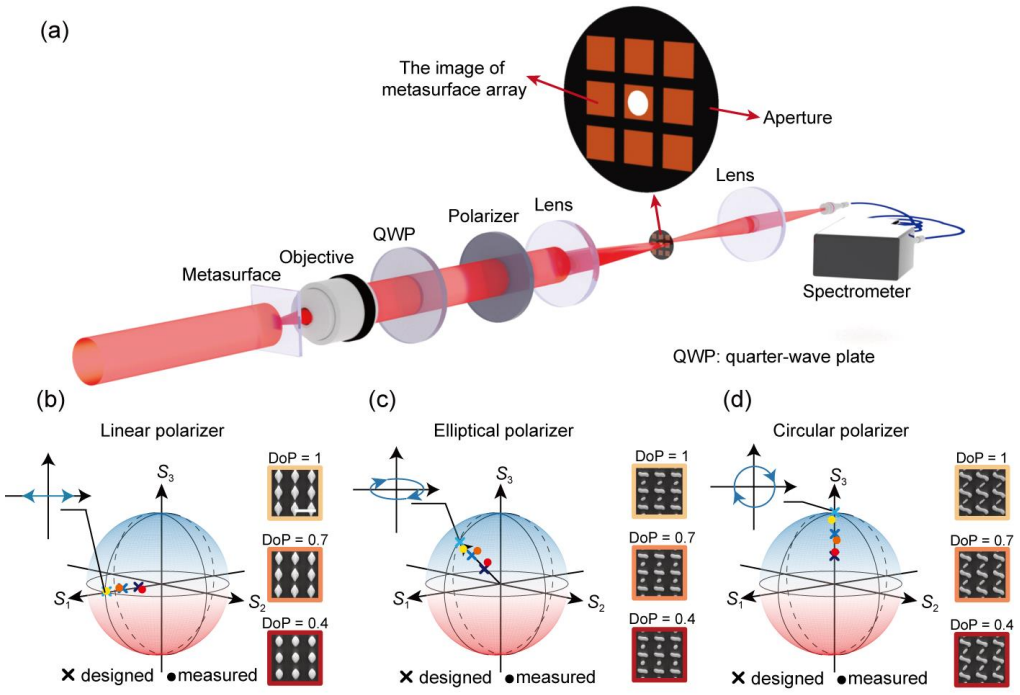

FIG. 4. Experimental demonstration of metasurface-based solid Poincaré sphere polarizers. (a) Experimental setup for the measurement of the Stokes parameter of light transmitted through the metasurface. (b)-(d) Comparison between the measured and designed Stokes parameters for the metasurface-based linear (b), elliptical (c), and circular (d) polarizer, respectively, each with a designed DoP of 1, 0.7, and 0.4, respectively. The inset shows the SEM images of fabricated metasurfaces. The scale bar is 1 μm.